Supplement to May / June 2024
Volume 53, Number 3

AppliedRadiology®

The Journal of Practical Medical Imaging and Management

Pediatric Imaging Case Series

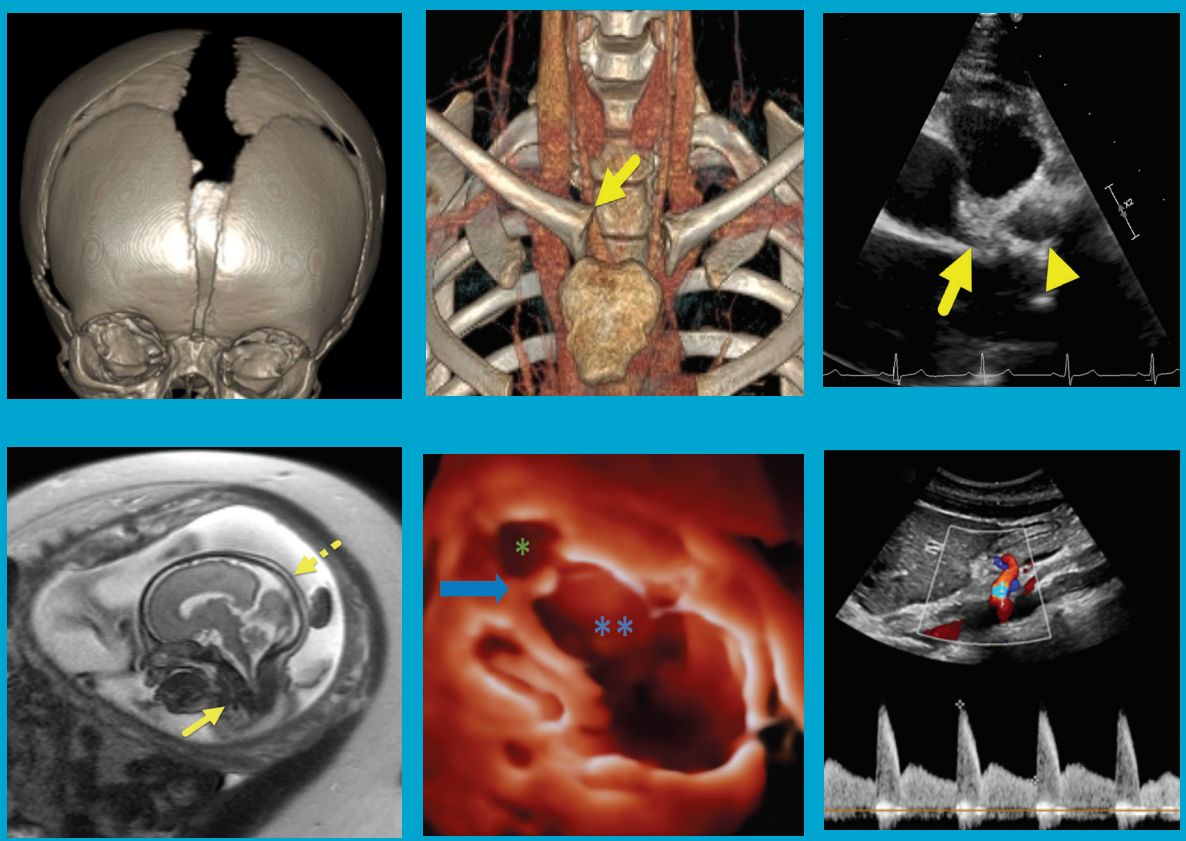

Choroid Plexus Papilloma | Sternoclavicular Physeal Separation | Kawasaki Disease

Congenital High Airway Obstruction Syndrome | Median Arcuate Ligament Syndrome | Ebstein Anomaly

Applied Radiology®

The Journal of Practical Medical Imaging and Management

Anderson Publishing, Ltd
180 Glenside Avenue,
Scotch Plains, NJ 07076
Tel: 908-301-1995
Fax: 908-301-1997
info@appliedradiology.com

Contents

Choroid Plexus Papilloma

Kalyani N. Ballur, BS; Richard B. Towbin, MD; Carrie M. Schaefer, MD; Daniel Morgan, DO; Alexander J. Towbin, MD

Case Summary

An infant presented with increased head circumference, a bulging anterior fontanelle, and a two-day history of downward gaze. Vital signs were significant for bradycardia with a heart rate of 78 bpm and hypertension with a systolic blood pressure of 161 mmHg. On examination, the pupils were 2 cm dilated and sluggish.

Imaging Findings

Noncontrast brain CT (Figure 1) showed a 3.2 x 3.7 cm intraventricular mass arising from the choroid plexus in the atrium of the left lateral ventricle. There was moderate hydrocephalus with transependymal CSF flow. Brain MRI (Figure 2) confirmed the intraventricular location of the tumor. On T1 and T2 images, the tumor was isointense with a central vascular pedicle. There was homogeneous contrast enhancement of the tumor. Vasogenic edema was present in the left occipital and posterior temporal lobes.

Diagnosis

Choroid plexus papilloma.

The differential diagnosis includes choroid plexus carcinoma, ependymoma, subependymoma, central neurocytoma, subependymal giant cell astrocytoma, and meningioma.

Discussion

Choroid plexus papillomas (CPPs) are benign tumors that arise from the choroid plexus epithelium.[1] They comprise 3% of intracranial tumors in the pediatric population, with 48% of patients diagnosed before 10 years and 20% before 1 year.[1] In children, CPPs most commonly arise within the lateral ventricles (64%) followed by the fourth (26%) and third ventricles (7%).[2] Tumors arising from other locations, such as the cerebellopontine angle, can occur but are rare.[2]

Patients typically present with signs and symptoms of increased intracranial pressure. These include headache, papilledema, vomiting, cranial nerve deficits, focal deficits, and seizures.[3] In infants, increasing head circumference, bulging fontanelle, lethargy, and fussiness are common.[1] The increased intracranial pressure is caused by hydrocephalus which results from cerebrospinal fluid (CSF) outflow obstruction and/or CSF overproduction.[1]

Choroid plexus tumors are classified by the World Health Organization (WHO) according to three grades based on histopathological findings: CPP (grade I); atypical CPP (grade II); and choroid plexus carcinoma (grade 3).[4] The atypical CPP was formally defined by the WHO in 2007 and can be histologically differentiated from a standard CPP by its increased cell density, nuclear pleomorphism, increased mitotic activity, and internal necrosis.[5]

On CT, CPP appears hypodense and lobular.[6] Approximately 25% of CPPs have internal calcifications and may appear cystic.[3] Owing to their highly vascular nature, the tumors enhance with contrast.[3] On MRI, they often appear cauliflower-shaped with an irregular contour and enhance with contrast.[3,7] On T1 MRI, CPP appears hypointense or isointense; on T2 images, it appears hyperintense.[4]

Calcifications appear hypointense whereas hemorrhage in the tumor may appear hyperintense, depending

Affiliations: Medical College of Georgia at Augusta University, Augusta, Georgia (Ms Ballur); Department of Radiology, Phoenix Childrens Hospital, Phoenix, Arizona (Drs Schaefer, R. Towbin); Children's Hospital Medical Center (Dr A. Towbin) and University of Cincinnati College of Medicine, Cincinnati, Ohio (Drs Morgan, A. Towbin)

Figure 1. (A) Axial noncontrast brain CT shows hydrocephalus and an isodense mass (arrow) arising from the glomus of the choroid plexus within the left lateral ventricle. (B) 3D reformatted surface rendering of the skull shows widening of the calvarial sutures and marked enlargement of the anterior fontanelle, secondary findings of increased intracranial pressure in an infant.

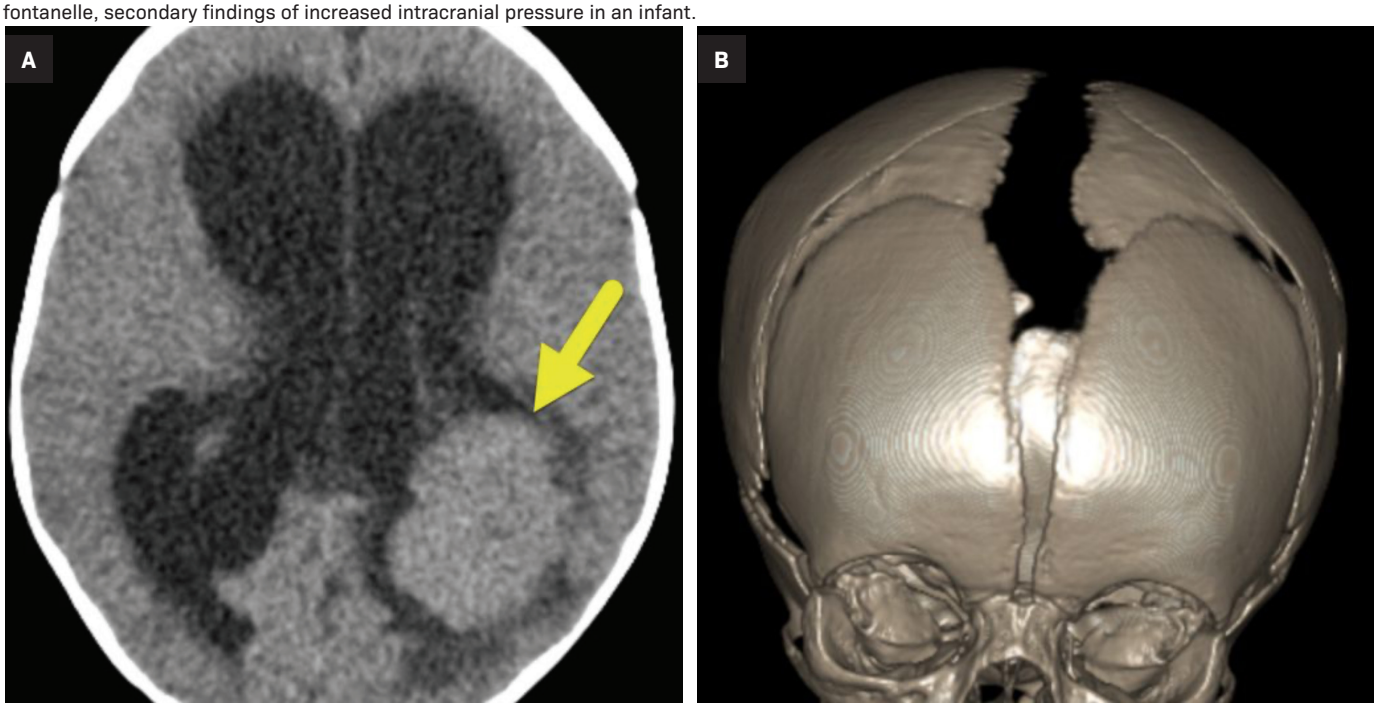

Figure 2. (A) Axial T1 MRI shows the lobulated, intermediate signal intensity mass (arrow) filling the atrium and occipital horn of the left lateral ventricle. (B) The mass (arrow) is relatively isointense to white matter on T2 images with the hypointense central vascular pedicle. Vasogenic edema is present in the occipital (short arrow) and posterior temporal lobes adjacent to the tumor. (C) On axial T1 postcontrast images, the tumor (arrow) enhances avidly.

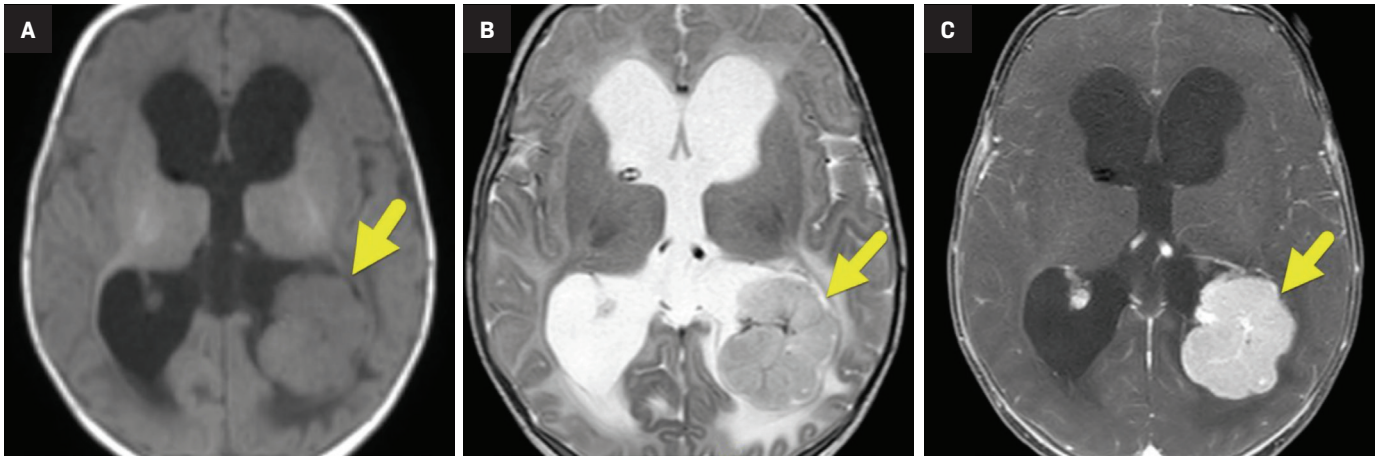

on its age.[3] MR angiography may provide information related to the vascular supply of the tumor, aiding surgical planning.[3] While the different types of choroid plexus tumors cannot be distinguished reliably via imaging, features such as large size, indistinct internal morphology, parenchymal invasion, peritumoral edema, and tumor necrosis increase the likelihood of malignancy.[8]

Patients with CPP typically have good outcomes after total surgical resection, with 5- and 10-year survival rates of 81% and 77%, respectively.[3,9] While CPPs are benign, they can recur after resection. Chemotherapy may be considered if the tumor is unresectable, recurs, or disseminates through the CSF.[3] Caution should be used in considering radiotherapy for children with CPP owing to the treatment's long-term consequences.[10] Hydrocephalus may persist after surgical resection due to adhesions in the subarachnoid spaces and/or occlusion of arachnoid granulation tissue.[7]

Conclusion

Choroid plexus papilloma is an uncommon, benign tumor typically found in the lateral ventricles. Diagnostic imaging is vital to identifying and planning surgery for this tumor, as complete surgical resection is the mainstay of treatment.

References

1) Kabashi A, Ahmetgjekaj I. Choroid plexus papilloma - case presentation. *Curr Health Sci J*. 2021;47(2):310-313. doi:10.12865/CHSJ.47.02.24

2) Wolff JE, Van Gool SW, Kutluk T,et al. Final results of the choroid plexus tumor study CPT-SIOP-2000. *J Neurooncol*. 2022;156(3):599-613. doi: 10.1007/s11060-021-03942-0.

3) Safaee M, Oh MC, Bloch O, et al. Choroid plexus papillomas: advances in molecular biology and understanding of tumorigenesis. *Neuro Oncol*. 2013;15(3):255-267. doi:10.1093/neuonc/nos289

4) Lin H, Leng X, Qin CH, Du YX, Wang WS, Qiu SJ. Choroid plexus tumours on MRI: similarities and distinctions in different grades. *Cancer Imaging*. 2019 Mar 20;19(1):17. doi: 10.1186/s40644-019-0200-1. PMID: 30894223; PMCID: PMC6427869.

5) Chen Y, Zhao R, Shi W, Li H. Pediatric atypical choroid plexus papilloma: Clinical features and diagnosis. *Clin Neurol Neurosurg*. 2021 Jan; 200:106345. doi: 10.1016/j.clineuro.2020.106345. *Epub* 2020 Nov 4. PMID: 33203591.

6) Sethi D, Arora R, Garg K, Tanwar P. Choroid plexus papilloma. *Asian J Neurosurg*. 2017;12(1):139-141. doi:10.4103/1793-5482.153501

7) Jaiswal AK, Jaiswal S, Sahu RN, Das KB, Jain VK, Behari S. Choroid plexus papilloma in children: Diagnostic and surgical considerations. *J Pediatr Neurosci*. 2009;4(1):10-16. doi:10.4103/1817-1745.49100

8) Lin H, Leng X, Qin CH, Du YX, Wang WS, Qiu SJ. Choroid plexus tumours on MRI: similarities and distinctions in different grades. *Cancer Imaging*. 2019;19(1):17. doi: 10.1186/s40644-019-0200-1.

9) Thomas C, Soschinski P, Zwaig M, et al. The genetic landscape of choroid plexus tumors in children and adults. *Neuro Oncol*. 2021;23(4):650-660. doi:10.1093/neuonc/noaa267

10) Wolff JE, Sajedi M, Brant R, Coppes MJ, Egeler RM. Choroid plexus tumours. *Br J Cancer*. 2002;87(10):1086-1091. doi: 10.1038/sj.bjc.6600609

Kawasaki Disease

Kaiden B. Porter; Richard B. Towbin, MD; Daniel Morgan, DO; Ryan A. Moore, MD; Carrie M. Schaefer, MD; Alexander J. Towbin, MD

Case Summary

An adolescent presented for follow up of aneurysms of the right coronary artery (RCA) and left anterior descending coronary artery (LAD). These were initially discovered when presenting as a baby with conjunctivitis, rash, skin desquamation, and diffuse erythema and swelling of the palms of the hands..

Imaging Findings

An echocardiogram (Figure 1) showed an aneurysm arising from the proximal LAD measuring 12 x 13.7 mm and another measuring 5.9 mm arising from the RCA.

Cardiac MRI (Figure 2) showed interval enlargement of the LAD aneurysm, with mural thrombus.

Cardiac catheterization (Figure 3) performed one year later showed no flow distal to the LAD aneurysm. Multiple collateral vessels were observed. Additionally, a new 9 mm aneurysm was present in the circumflex artery. The aneurysm arising from the RCA had enlarged considerably. The remainder of the vessel was tortuous, and a stenosis was suggested. The findings were confirmed on CT angiography (Figure 4).

Diagnosis

Kawasaki disease with coronary artery aneurysms.

Discussion

Kawasaki disease (KD) is an inflammatory condition that primarily affects small to medium-sized blood vessels in children under 5 years old, more common in boys. It is the leading cause of acquired heart conditions in children from developed nations.[1] Although the cause of the disease is unknown, various theories center on its pathogenesis. These include an unknown, seasonal, airborne infectious agent or genetic abnormalities such as changes in *caspase 3, inositol 1,4,5, trisphosphate kinase C, DC40, FCGR2a,* and B cell lymphoid kinase that increase the risk of KD. The infectious and seasonal etiologies are supported primarily by clusters of epidemics that seem to have followed wind patterns occurring in Eastern Asia and several Western countries. The genetic theory is supported by variations associated with KD development, prognosis, and coronary artery aneurysm development.[2]

The epidemiology of KD is highly dependent on geographic location and ethnicity. The highest incidence of KD occurs in Japan, where 264 per 100,000 children are affected. This high incidence raises awareness and the associated mortality rate in Japan is less than 0.02%.[2] In the continental United States, the incidence is notably lower, affecting 13-21 children per 100,000.[2,3]

Kawasaki disease is diagnosed on the basis of five clinical signs: 1) mucocutaneous changes such as erythema of the tongue (ie, “strawberry tongue”) and severe cheilitis (lip swelling and cracking); 2) nonexudative conjunctivitis with limbic sparing; 3) a polymorphous rash; 4) extremity changes such as edema and periungual desquamation; and 5) cervical lymphadenopathy.[1,3,4]

Patients must exhibit a fever for ≥ 5 days and at least four of the above signs for KD to be diagnosed. Other notable potential cardiac complications include myocarditis, valvular

Affiliations: University of Arizona College of Medicine-Phoenix Campus, Phoenix, Arizona (Mr Porter); Department of Radiology, Phoenix Children’s Hospital, Phoenix, Arizona (Drs Schaefer, R. Towbin); Department of Radiology, University of Cincinnati College of Medicine (Drs Morgan, Dr A. Towbin) and Department of Radiology, Cincinnati Children’s Hospital (Dr A. Towbin), Department of Pediatrics, Division of Cardiology, Cincinnati Children’s Hospital, Cincinnati, Ohio (Dr Moore).

Figure 1. Echocardiogram shows (A) an aneurysm (arrowhead) arising from the proximal aspect of the LAD coronary artery near the origin of the left main coronary artery (arrow). (B) A smaller fusiform aneurysm (arrow) is present at the origin of the RCA.

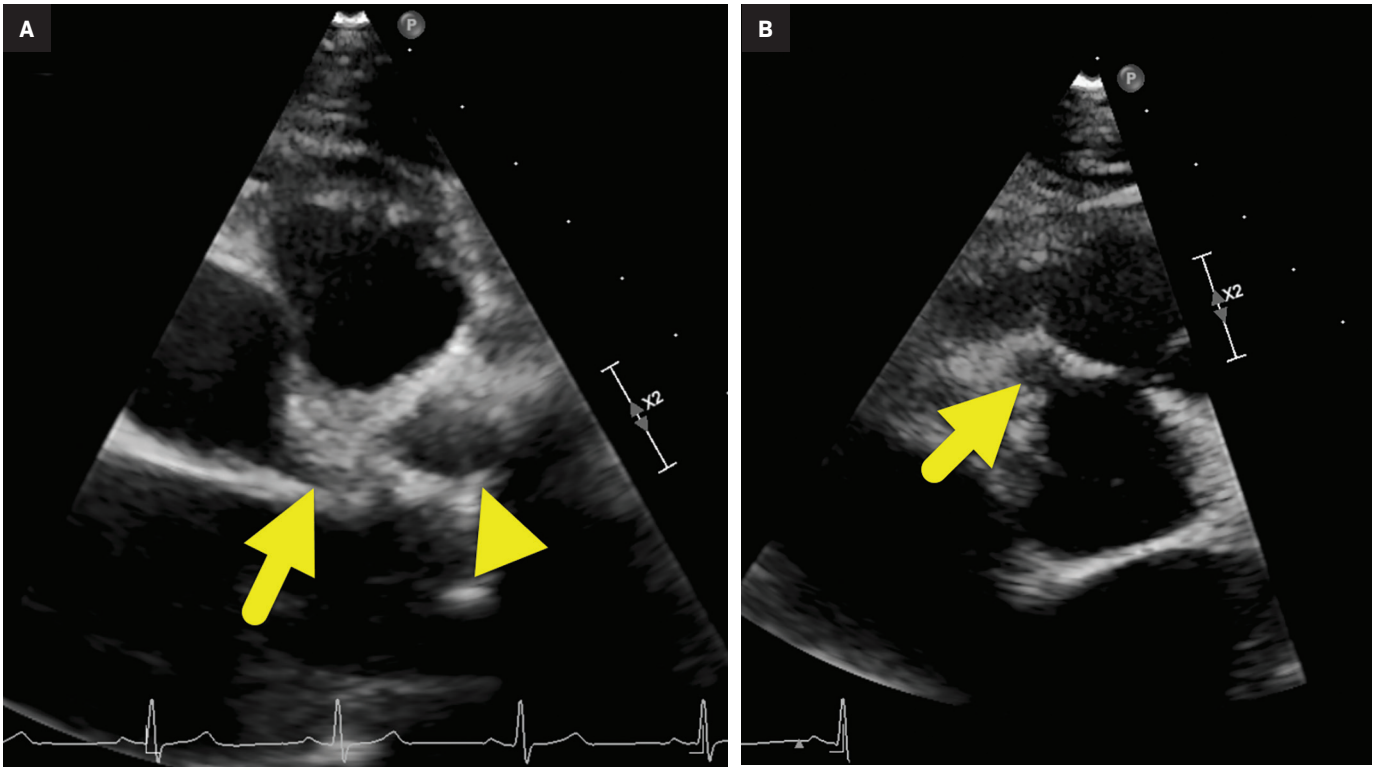

Figure 2. Coronal 3D balanced turbo field echo sequence cardiac MRI demonstrates a largely thrombosed aneurysm (arrowhead) arising from the proximal aspect of the LAD coronary artery near the origin of the left main coronary artery (arrow).

regurgitation, and coronary artery abnormalities. Incomplete (atypical) KD occurs when not all classic KD criteria are met; however, the children remain at risk for cardiovascular complications.[5] Kawasaki disease is most often diagnosed when screening echocardiography reveals dilated coronary arteries. Patients with incomplete KD will often follow the same clinical course as classic KD.

Kawasaki disease generally presents in three phases: acute (1-2 weeks); subacute (2-4 weeks); and convalescent (4-8) weeks.[4] The acute phase is associated with a high fever and the classic symptoms listed above. The subacute phase is usually asymptomatic. During this phase, the patient is at high risk of developing associated cardiac complications such as coronary artery dilation and subsequent aneurysm formation. Approximately 25% of untreated and 5% of treated patients will develop coronary abnormalities.

Figure 3. Cardiac catheterization (A) aortogram shows an aneurysm (arrow) of the LAD coronary artery. The larger, thrombosed portion of the aneurysm (arrowhead) is partially calcified. There is no flow in the more distal portion of the vessel. A fusiform aneurysm (dashed arrow) arises from a branch of the left circumflex coronary artery. (B) Left main coronary artery injection highlights the same aneurysm (arrow) of the LAD coronary artery, thrombosed portion of the aneurysm (arrowhead), and fusiform aneurysm (dashed arrow) of the left circumflex coronary artery. (C) RCA injection shows an aneurysm (arrow).

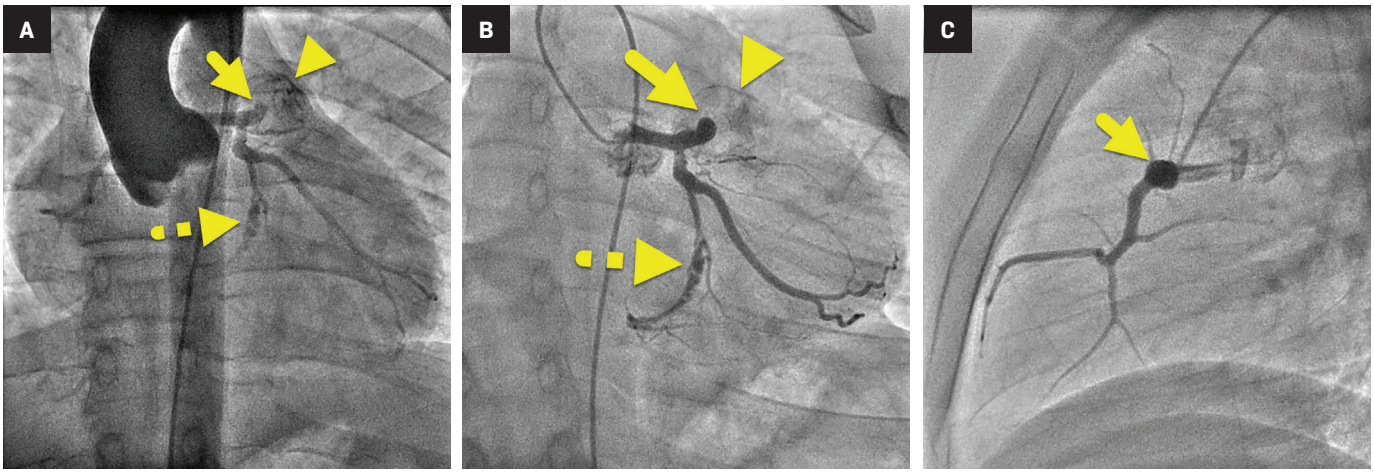

Figure 4. Cardiac CT axial maximum intensity projection image at the level of (A) the left main coronary artery and (B) the right main coronary artery shows a thrombosed aneurysm (arrowhead) at the origin of the LAD coronary artery and a fusiform aneurysm (arrow) of the RCA. (C) 3D reconstructed image shows an aneurysm (arrowhead) of the left anterior descending coronary artery. Fusiform aneurysms are present arising from a branch of the left circumflex coronary artery (dashed arrow) and right coronary artery (arrow).

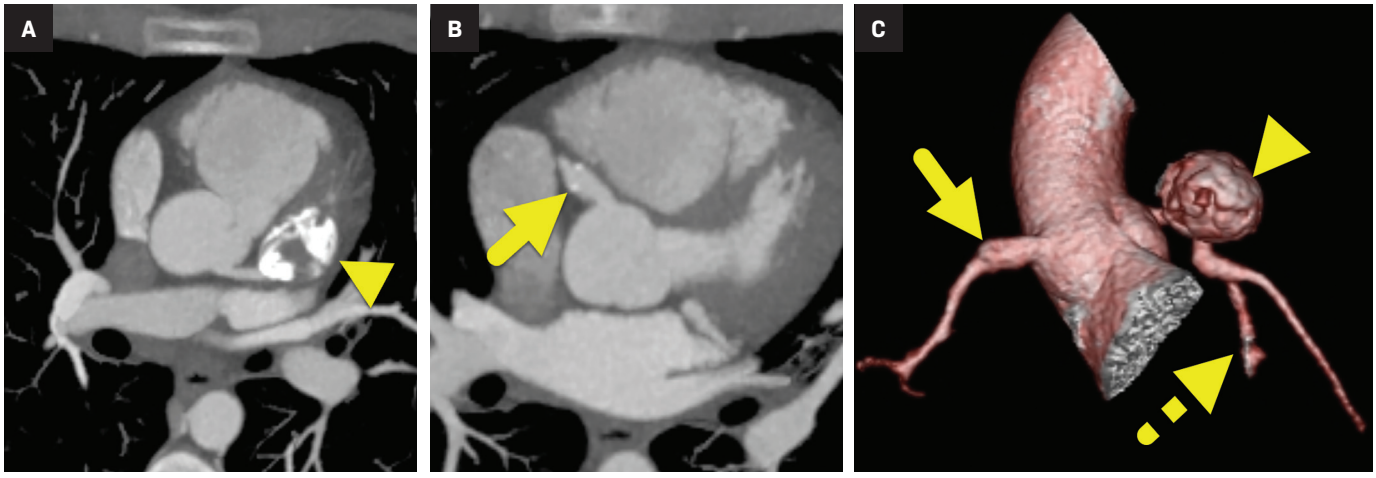

The convalescent phase is also usually asymptomatic, but patients are now at a lower risk for developing cardiac symptoms owing to increased surveillance (including close clinical monitoring for fever recurrence) and a low threshold for treatment.

Laboratory findings, though nonspecific, can aid in making the diagnosis. Children can present with neutrophilia > 15,000 per mm;[3] anemia; thrombocytosis > 450,000 per mm;[3] and elevated ferritin, ALT, GGT, ESR, and C-reactive protein. Sterile pyuria of >10 WBCs per high powered field may also occur.[5]

During all phases of KD, imaging is used to detect potential cardiac anomalies. Echocardiography remains the imaging modality of choice.[4] It is performed at the time of suspected KD diagnosis, up to 14 days later, and 6-8 weeks after that to survey for any cardiac abnormalities. If they are observed, imaging can be used for a longer duration to assess severity and prognosis.

Other potential studies that can be valuable are MR angiography, CT angiography, and cardiac catheterization. Cardiac catheterization may be warranted if coronary artery aneurysms are suspected.

Kawasaki disease is treated with intravenous immunoglobulin (IVIG) at a dose of 2 g/kg. Ideally, children should be treated within 10 days of the onset of fever. Effective IVIG therapy reduces the risk of a coronary artery lesion from 20-25% to 3-5%. However, up to 20% of patients will be termed “IVIG-resistant” and will experience recurrent fevers. A moderate dose (30-50 mg/kg/day)

of acetylsalicylic acid (ASA) is also given. In Japan and the United States, treatment with ASA is continued until the fever abates.[6]

Patients with coronary artery aneurysms are also treated with antithrombotic agents. The medication used is dependent on the size of the lesion. Patients with small aneurysms are continued on ASA for a period after the initial 6–8-week treatment regimen. Patients with aneurysms with an internal diameter >8 mm are generally started on anticoagulant therapy with warfarin or low molecular weight heparin.[6]

Conclusion

Kawasaki disease is an inflammatory vasculitis that primarily affects small to medium-sized vessels and is predominantly seen in male children under the age of 5 years. Those of Japanese ethnicity are at highest risk for the condition, which is associated with mucosal changes such as erythema and "strawberry tongue," conjunctivitis, a polymorphous rash, extremity changes such as edema and periungual desquamation, and lymphadenopathy.

Coronary artery aneurysms are the feared sequelae of KD. Echocardiography is frequently used to assess for aneurysm development. The diseaes are generally treated with IVIG and ASA. Patients with aneurysms with an internal diameter greater than 8 mm are also treated with anticoagulant therapy.

References

1) Singh, S., Jindal, A. K., & Pilania, R. K. (2018). Diagnosis of Kawasaki disease. *Int J Rheum Dis.*, *21*(1):36–44. doi:10.1111/1756-185X.13224. *Epub* 2017 Nov 13. PMID: 29131549; PMCID: PMC7159575.

2) Elakabawi K, Lin J, Jiao F, Guo N, Yuan Z. Kawasaki Disease: global burden and genetic background. *Cardiol Res.* 2020 Feb;11(1):9-14. doi: 10.14740/cr993. *Epub* 2020 Jan 26. PMID: 32095191; PMCID: PMC7011927.

3) Harnden A, Takahashi M, Burgner D. Kawasaki disease. *BMJ.* 2009 May 5;338: b1514. doi: 10.1136/bmj. b1514. PMID: 19416993.

4) Vervoort D, Donné M, Van Gysel D. Pitfalls in the diagnosis and management of Kawasaki disease: An update for the pediatric dermatologist. *Pediatr Dermatol.* 2018 Nov;35(6):743-747. doi: 10.1111/pde.13620. *Epub* 2018 Oct 18. PMID: 30338568.

5) Rowley, A. H. (2015). The complexities of the diagnosis and management of Kawasaki disease. Infectious disease clinics of North America, 29(3), 525537. https://doi.org/10.1016/j.idc.2015.05.006

6) Rife E, Gedalia A. Kawasaki disease: an update. *Curr Rheumatol Rep.* 2020 Sep 13;22(10):75. doi: 10.1007/s11926-020-00941-4. PMID: 32924089; PMCID: PMC7487199.

Congenital High Airway Obstruction Syndrome

Nisha Rehman; Richard B. Towbin, MD; Carrie M. Schaefer, MD; Alexander J. Towbin, MD

Case Summary

A screening obstetrical ultrasound performed at 29 weeks' gestation demonstrated polyhydramnios with an amniotic fluid index (AFI) of 27.1cm (normal 10.5-18.9). Several abnormalities were present in the fetus, including shortened long bones, mesocardia with enlarged lungs, and massive ascites. A diagnostic fetal ultrasound and a fetal MRI were performed.

Imaging Findings

Fetal ultrasound (Figure 1) showed enlarged, echogenic lungs, mesocardia, a dilated fluid-filled trachea, and marked ascites. Fetal MRI (Figure 2) failed to demonstrate a cervical tracheal fluid column and confirmed the dilated, fluid-filled thoracic trachea, enlarged lungs causing mass effect upon the cardiomediastinal structures and eversion of the diaphragm, and fetal hydrops.

Diagnosis

Congenital high airway obstruction sequence (CHAOS)

Discussion

CHAOS is a rare proximal congenital airway obstruction that leads to distal airway dilatation, expanded lungs with mass effect on the heart, ascites, and hydrops.[1] The condition is characterized by partial or complete obstruction of the upper airway. The obstruction can vary in location and severity. Types of obstruction include laryngeal atresia (the most common), laryngeal stenosis and dysgenesis, subglottic stenosis, tracheal aplasia, and tracheal stenosis.[2]

If the condition goes unrecognized in utero, the fetus does not usually survive. However, if an ex-utero intrapartum treatment (EXIT) procedure is performed, survival can occur but depends on the associated congenital anomalies.

CHAOS is predominantly sporadic.[3] However, it can be seen in syndromes such as Fraser, cri-du-chat, short-rib polydactyly, and velocardiofacial (DiGeorge syndrome).[4,5] Thus, a fetus with CHAOS should be evaluated for other anomalies that may be part of a genetic syndrome.

CHAOS is diagnosed via prenatal imaging. The initial imaging study of choice is fetal ultrasound. Typical findings include enlarged hyperechoic lungs, dilated fluid-filled airways, a compressed and centrally positioned heart, flattened/inverted diaphragms, ascites, hydrops, and polyhydramnios.[6,7] Guimaraes et al recommend that the presence of these signs prompt consideration of genetic counseling and fetal MRI. The modality can demonstrate increased lung volumes with flattened or inverted hemidiaphragms, a dilated airway below the level of obstruction, massive ascites, mesocardiac, and placentomegaly, in which the placenta is disproportionately large or thicker than 4 cm.[8]

Improvements in prenatal imaging and treatment modalities have led to increased survival in fetuses with CHAOS. Prenatally, treatment can include amnioreduction.[9] While there are a small number of reports of spontaneous resolution of CHAOS,[9] the initial intervention is the EXIT procedure, which allows surgeons to secure an airway, commonly in the form of a tracheostomy, below the obstruction.[9] After birth, the airway obstruction is definitively treated via surgery. More recently, an in-utero treatment has been developed that relies on fetoscopic, ultrasound-guided decompression of the laryngeal atresia. In this technique a wire is passed across the atretic region of the airway. This is followed by balloon dilation of the airway with stent placement and laser laryngotomy.[9]

Conclusion

CHAOS is characterized by the partial or complete obstruction of the fetal upper airway that can occur sporadically or as part of a syndrome. Fetal imaging is a mainstay of diagnosis and management of the condition. Advances in imaging and treatment may reduce neonatal mortality.

References

1) Hedrick M, Ferro M, Filly R, Flake A, Harrison M, Scott Adzick N. Congenital high airway obstruction syndrome (CHAOS): A potential for perinatal intervention. *J Pediatr Surg*. 1994;29(2):271-274. doi:10.1016/0022-3468(94)90331-x

Affiliations: University of Arizona College of Medicine-Phoenix Campus, Phoenix, Arizona (Ms Rehman); Department of Radiology, Phoenix Children's Hospital, Phoenix, Arizona Drs Schaefer, R. Towbin); Department of Radiology, Cincinnati Children's Hospital and University of Cincinnati College of Medicine, Cincinnati, Ohio (Dr A. Towbin).

Figure 1. (A) Axial ultrasound through the fetal chest at 29 weeks' gestation demonstrates markedly enlarged, echogenic lungs and mesocardia. (B) Longitudinal ultrasound of the fetal chest and abdomen demonstrates the dilated lower trachea (arrow), surrounded by echogenic lungs, and the marked ascites.

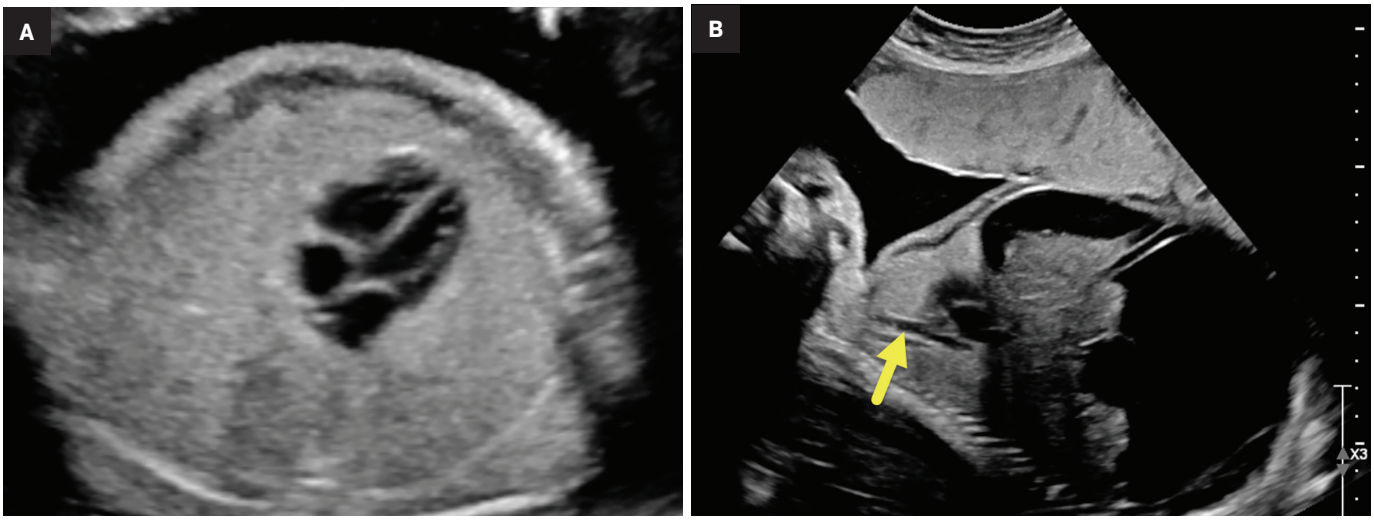

Figure 2. (A) MRI of the fetal brain and neck demarcates the atresia (arrow) of the cervical trachea indicated by the absence of fluid signal. Scalp edema (dashed arrow) results from the hydrops. (B) MRI obliquely through the fetal chest and abdomen demonstrates the dilated thoracic trachea (arrow), enlarged lung, eversion of the diaphragm, marked ascites, and skin edema (dashed arrow) from hydrops.

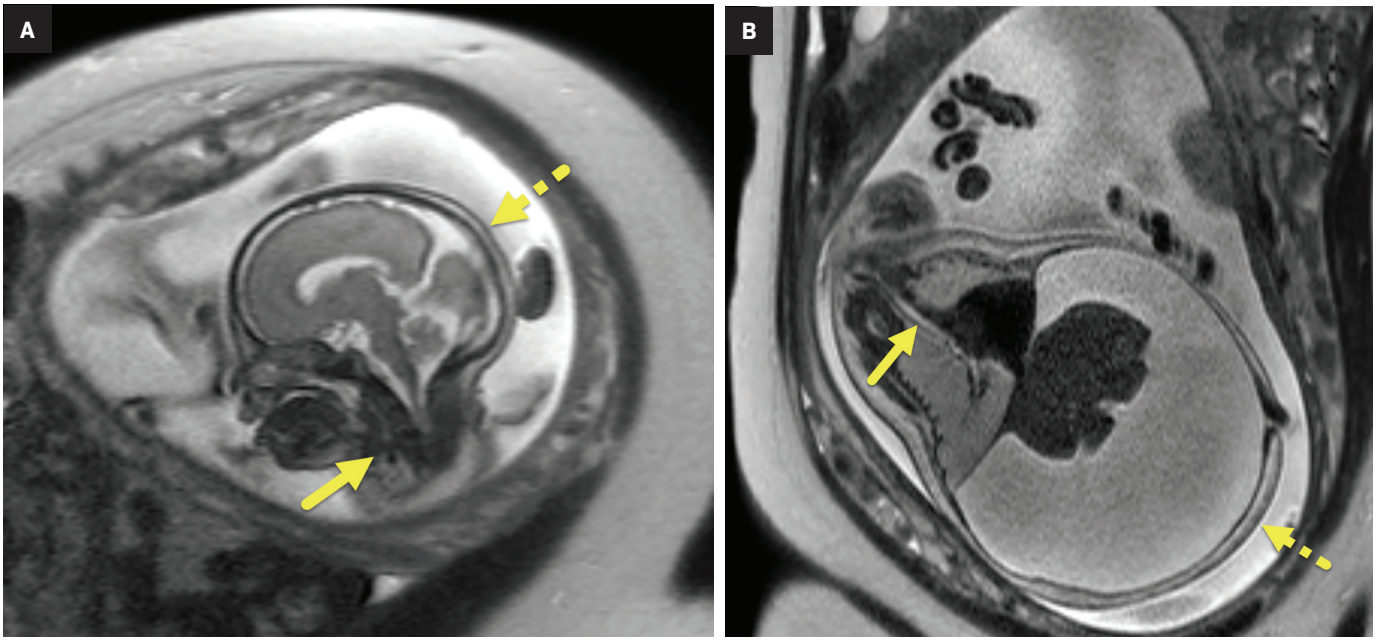

2) Sanford E, Saadai P, Lee H, Slavotinek A. Congenital high airway obstruction sequence (CHAOS): A new case and a review of phenotypic features. *Am J Med Genetics Part A*. 2012;158A (12):3126-3136. doi:10.1002/ajmg.a.35643

3) Vanhaesebrouck P, De Coen K, Defoort P, et al. Evidence for autosomal dominant inheritance in prenatally diagnosed CHAOS. *Eur J Pediatr*. 2006;165(10):706-708. doi:10.1007/s00431-006-0134-z

4) Joshi P, Satija L, George R, Chatterjee S, D'Souza J, Raheem A. Congenital high airway obstruction syndrome-antenatal diagnosis of a rare case of airway obstruction using multimodality imaging. *Med J Armed Forces India*. 2012;68(1):78-80. doi:10.1016/S0377-1237(11)60111-1

5) Lim FY, Crombleholme TM, Hedrick HL, et al. Congenital high airway obstruction syndrome: natural history and management. *J Pediatr Surg*. 2003;38(6):940-945. doi:10.1016/s0022-3468(03)00128-3

6) Mudaliyar US, Sreedhar S. Chaos syndrome. *BJR Case Rep*. 2017;3(3): 20160046. doi:10.1259/bjrcr.20160046

7) Garg MK. Case report: Antenatal diagnosis of congenital high airway obstruction syndrome - laryngeal atresia. *Indian J Radiol Imaging*. 2008;18(4):350-351. doi:10.4103/0971-3026.43843

8) Guimaraes CV, Linam LE, Kline-Fath BM, et al. Prenatal MRI findings of fetuses with congenital high airway obstruction sequence. *Korean J Radiol*. 2009;10(2):129-134. doi:10.3348/kjr.2009.10.2.129

9) Nolan H, Gurria J, Peiro J et al. Congenital high airway obstruction syndrome (CHAOS): Natural history, prenatal management strategies, and outcomes at a single comprehensive fetal center. *J Pediatr Surg*. 2019;54(6):1153-1158. doi: 10.1016/j.jpedsurg.2019.02.03

Ebstein Anomaly

Mark A. Sanders; Richard B. Towbin, MD; Carrie M. Schaefer, MD; Alexander J. Towbin, MD

Case Summary

A pregnant patient with a previous infant with Ebstein anomaly (EA) and Trisomy 21 underwent a fetal echocardiogram. The current fetus's echocardiogram at 25 weeks' gestation demonstrated apical displacement of the tricuspid valve and a hypoplastic right ventricle.

Imaging Findings

Fetal MRI at 32 weeks 3 days' gestation demonstrates a markedly enlarged right atrium and atrialized right ventricle. Fetal 4D echocardiogram (Figure) on the same day demonstrated apical displacement of the septal leaflet of the tricuspid valve, marked dilatation of the right atrium, and atrialization of the right ventricle.

Diagnosis

Ebstein anomaly.

The differential diagnosis includes Uhl anomaly, tricuspid valve dysplasia or prolapse, pulmonary valve stenosis, Tetralogy of Fallot, and arrhythmogenic right ventricular cardiomyopathy.

Affiliations: Kaiser Permanente School of Medicine, Pasadena, California (Mr Sanders); Department of Radiology, Phoenix Children's Hospital, Phoenix, Arizona (Drs Schaefer, R. Towbin); Department of Radiology, Cincinnati Children's Hospital; Department of Radiology, University of Cincinnati College of Medicine, Cincinnati, Ohio (Dr A. Towbin).

Discussion

Ebstein anomaly is a congenital, right-sided cardiomyopathy characterized by tricuspid valve displacement inferiorly into the right ventricle. It is a rare condition, accounting for 1% of all congenital heart disease.[1] While most cases are sporadic, EA has been linked to isolated genetic defects and prenatal lithium exposure.[2]

Ebstein anomaly is caused by incomplete separation of the septal and posterior leaflets of the tricuspid valve from the underlying myocardium during development. Because the valves fail to separate, they remain attached to the myocardium and are displaced downward, resulting in "atrialization" of the right ventricle.

The atrialized portion of the right ventricle is above the septal and posterior tricuspid valve leaflets and consists of the inlet component of the malformation, which is dilated and contiguous with the right atrium. This ultimately leads to a reduced ventricular volume, decreased right ventricular function, tricuspid regurgitation, right atrial dilation, cardiomegaly, and right heart failure.[3]

In addition to being regurgitant, the tricuspid valve also has abnormal morphology. The anterior tricuspid leaflet bulges in a sail-like configuration, obstructing right ventricular outflow. This right ventricular outflow obstruction leads to right-to-left shunting, often through a patent foramen ovale or atrial septal defect.[4]

The clinical presentation of EA varies, depending on the severity of the abnormality, and ranges from asymptomatic with mild atrial displacement to heart failure and death. Features that prompt evaluation for EA include hydrops fetalis and tachyarrhythmias on prenatal ultrasound, cyanosis or heart murmur in neonates and children, and arrythmias or signs of right heart failure in adults.[3]

Ebstein anomaly is often diagnosed in utero. Routine prenatal ultrasound may show cardiomegaly, tachyarrhythmias, or hydrops fetalis.[5] After birth, chest radiograph is often the initial imaging study performed, demonstrating cardiomegaly with a "box-shaped heart" resulting from right atrial enlargement. Ebstein anomaly is also the most common cause of massive cardiomegaly, giving the heart a "wall-to-wall" appearance, touching both the right and left lateral chest walls.

After birth, EA is diagnosed via echocardiography or, if inconclusive, cardiac MRI. Findings include apical displacement of the septal leaflet of the tricuspid valve and an elongated, sail-like anterior tricuspid valve leaflet.[3] Echocardiography can determine the severity of EA via the extent of tricuspid regurgitation, through measurements of regurgitant flow velocity and jet area.

Figure. (A) Fetal 4D echocardiogram during diastole demonstrating the presence of a markedly dilated right atrium and atrialized right ventricle (*) due to apical displacement of the septal leaflet of the tricuspid valve (arrow), which is thickened. The right ventricle (**) is hypoplastic. (B) Fetal 4D echocardiogram during systole demonstrating the closed, dysplastic tricuspid valve (*) and patent foramen ovale (**). Right atrium (RA).

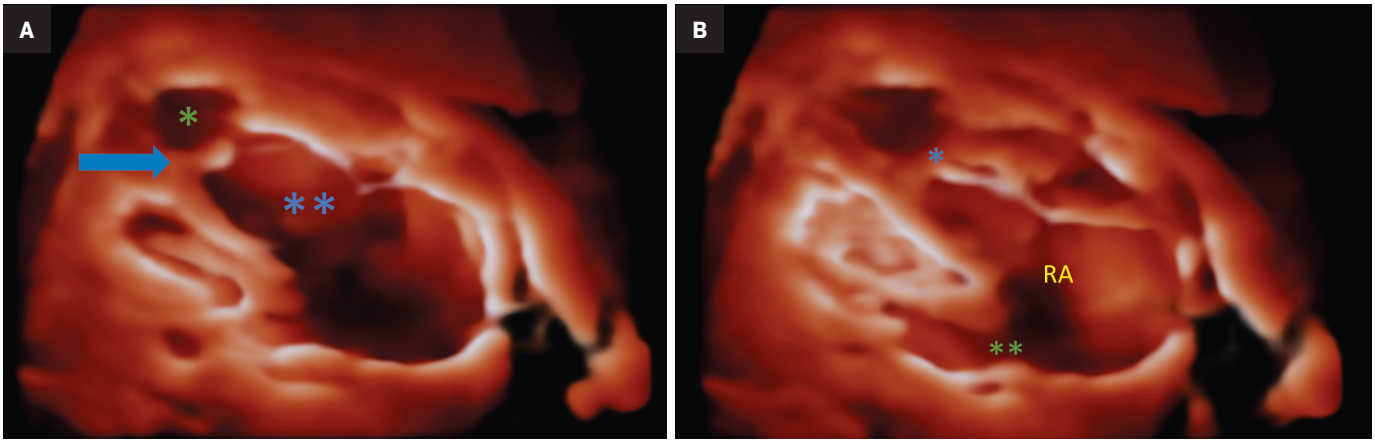

The Great Ormond Street Echo (GOSE) score provides prognostic information by predicting the risk of death. The GOSE score is calculated by determining the ratio of the area of the right atrium and atrialized right ventricle to the area of the remaining three cardiac chambers on a standard four-chamber view.[6] A GOSE score ≥ 1.5 is uniformly fatal, while scores < 1 have an 8% risk of mortality.[7] Cardiac MRI can offer better quantification of EA and has been used to confirm the diagnosis and to grade severity. In today's practice it is used prior to surgical intervention.[8]

Once the condition is diagnosed, patients should typically undergo monitoring every 1-2 years with exercise tolerance testing, an electrocardiogram, and cardiac MRI to assess for new signs and symptoms, arrythmias, and progression of cardiac dysfunction.[9] Surgical repair is often performed in symptomatic children and adults. Options include tricuspid valve replacement or valvuloplasty, atrialized right ventricle plication, right reduction arterioplasty, and any necessary corrections of arrhythmias or cardiac shunts.[10]

Prognosis varies with patient age and EA severity. When the condition is diagnosed during the prenatal or neonatal period, prognosis is typically poor with a 30% 1-year mortality rate. Neonates who are cyanotic have a worse prognosis. For example, acyanotic patients with a GOSE Score ratio of 1.1-1.49 have a 10% early mortality rate. This differs from cyanotic patients with the same GOSE Score ratio who have a 100% mortality rate.[7] Patients with less-severe disease may be diagnosed in adolescence or early adulthood. These patients have a 20% risk of death by 30 years of age.[1]

Conclusion

Ebstein anomaly is a rare, congenital, right-sided cardiomyopathy that is characterized by tricuspid valve displacement inferiorly into the right ventricle, resulting in tricuspid regurgitation and eventual right heart failure. The etiology is multifactorial, and most cases are sporadic, with prenatal lithium exposure and isolated genetic defects also being implicated.

Diagnosis is confirmed on echocardiography or cardiac MRI. Ebstein anomaly is managed medically until surgical repair can be performed, and the prognosis is dependent on patient age and symptoms.

References

1) Lupo PJ, Langlois PH, Mitchell LE. Epidemiology of Ebstein anomaly: prevalence and patterns in Texas, 1999-2005. *Am J Med Genet A*. 2011; (5):1007-1014. doi: 10.1002/ajmg.a.33883. *Epub* 2011 Apr 4. PMID: 21465650.

2) Patorno E, Huybrechts KF, Bateman BT, Cohen JM, Desai RJ, Mogun H, Cohen LS, Hernandez-Diaz S. Lithium use inpregnancy and the rsk of cardiac malformations. *N Engl J Med*. 2017;;376(23):2245-2254. doi: 10.1056/NEJMoa1612222. PMID: 28591541; PMCID: PMC5667676.

3) Jost CHA, Connolly HM, Dearani JA, Edwards WD, Danielson GK. Ebstein's anomaly. *Circulation*. Published online 2007. doi:10.1161/CIRCULATIONAHA.106.619338

4) Attenhofer Jost CH, Connolly HM, Dearani JA, Edwards WD, Danielson GK. Ebstein's anomaly. *Circulation*. 2007;16;115(2):277-285. doi: 10.1161/CIRCULATIONAHA.106.619338. PMID: 1722801

5) Celermajer DS, Bull C, Till JA, et al. Ebstein's anomaly: presentation and outcome from fetus to adult. *J Am Coll Cardiol*. 1994;(1):170-176. doi: 10.1016/0735-1097(94)90516-9. PMID: 8277076.

6) Celermajer DS, Bull C, Till JA, et al. Ebstein's anomaly: presentation and outcome from fetus to adult. *J Am Coll Cardiol*. 1994;23(1):170-176. doi: 10.1016/0735-1097(94)90516-9. PMID: 8277076.

7) Knott-Craig, CJ, Boston US. Current surgical techniques in the management of the symptomatic neonate with severe Ebstein anomaly: Too much, too little, or just enough? *JTCVS Techniques*. Published online 2021. https://doi.org/10.1016/j.xjtc.2021.05.030

8) Geerdink LM, van Everdingen WM, Kuipers IM, et al. Comprehensive evaluation of pediatric patients with Ebstein anomaly requires both echocardiography and cardiac magnetic resonance imaging. *Pediatr Cardiol*. 2023;(1):75-85. doi: 10.1007/s00246-022-02948-3. Epub 2022 Jun 21. PMID: 35727332; PMCID: PMC9852135.

9) Stout KK, Daniels CJ, Aboulhosn JA, et al. 2018 AHA/ACC Guideline for the Management of Adults With Congenital Heart Disease: A Report of the American College of Cardiology/American Heart Association Task Force on Clinical Practice Guidelines. *Circulation*. Published online 2019. doi:10.1161/CIR.0000000000000603

10) Dearani JA, Mora BN, Nelson TJ, Haile DT, O'Leary PW. Ebstein anomaly review: What's now, what's next? *Expert Rev Cardiovasc Ther*. Published online 2015. doi:10.1586/14779072.2015.1087849

Median Arcuate Ligament Syndrome

Josh Theis; Carrie M. Schaefer, MD; Alexander J. Towbin, MD; Richard B. Towbin, MD

Case Summary

An adolescent with a two-year history of abdominal pain and vomiting after meals presented with diffuse abdominal tenderness on palpation. The diagnostic workup consisted of a normal upper gastrointestinal series and esophagogastroduodenoscopy, as well as a celiac nerve block which did not relieve the postprandial pain. Subsequently, the patient underwent a surgical division of the median arcuate ligament (MAL), with resultant decreased intensity and frequency of the postprandial pain and vomiting.

Imaging Findings

Abdominal ultrasound (US) of the aorta and celiac axis during inspiration and expiration (Figure 1) demonstrated a narrowed celiac origin on inspiration and a "hooked" appearance of the celiac origin with expiration. Duplex Doppler US images on inspiration and expiration demonstrated an abnormally increased peak systolic velocity of 318 cm/sec (normal < 200cm/second) during expiration and a deflection angle > 50 degrees (Normal < 50 degrees). An abdominal CT angiogram (Figure 2) with 3D reconstruction revealed arterial narrowing at the origin of the celiac axis with post stenotic dilatation.

Diagnosis

Median arcuate ligament syndrome.

The differential diagnosis includes gastritis, Crohn disease, inflammatory bowel syndrome, peptic ulcer disease, and gastroesophageal reflux disease (GERD).

Discussion

Median arcuate ligament syndrome (MALS), also known as Dunbar Syndrome, is an uncommon condition where the MAL compresses the celiac trunk. The condition was first discovered in 1917 by Benjamin Lipshutz while dissecting cadavers; he noted the MAL overlapping and compressing the celiac artery.[1] Many cases of MALS are asymptomatic, owing to typically minor compression and/or development of collateral circulation, especially involving the arterial arcades of the pancreas.[2] In symptomatic cases, the symptoms are often attributed to other abdominal pathologies. It is usually diagnosed after other etiologies have been excluded. MALS typically affects women 20-40 years of age, most commonly at a ratio of 2:1 or 3:1 that of the general population. The incidence of MALS is approximately 2 per 100,000.[3]

As the first major branch of the descending abdominal aorta, the celiac artery usually originates just below the crus of the diaphragm. The vessel supplies blood to the liver, stomach, abdominal esophagus, spleen, and the superior portions of the duodenum and the pancreas. The MAL crosses over the aorta just above the celiac trunk, with its primary role to attach the diaphragm to the spine.

In patients with MALS, the ligament is lower than normal, compressing the celiac trunk and reducing blood flow to the abdominal organs, especially the stomach and liver.[4] This hypoperfusion leads to many of the manifestations of MALS, which may rarely even include necrosis of the stomach and liver if left untreated.[5] The most prevalent signs and symptoms are postprandial nausea, diarrhea, vomiting, and food aversion. In addition, a bruit may be present in the epigastric region. Food aversion often leads to significant weight loss, typically more than 20 pounds.

The pain is believed to be caused by compression of the celiac plexus, the collection of nerves located directly over the celiac artery.[6]

Other common etiologies such as GERD, gastritis, and Crohn disease must first be excluded before MALS can be diagnosed. Patients in suspect cases will undergo Doppler ultrasound and CT examination.[7] In those with MALS, Doppler ultrasound of the celiac artery will reveal lower

Affiliations: University of Arizona College of Medicine-Phoenix Campus (Mr Theis); Department of Radiology, Phoenix Children's Hospital, Phoenix, Arizona (Drs Schaefer, R Towbin); Children's Hospital Medical Center, Cincinnati, and University of Cincinnati College of Medicine (Dr A Towbin).

Figure 1. Ultrasound of the abdominal aorta at the level of the celiac axis during inspiration (A) shows a narrowed celiac origin on inspiration (arow) and during expiration (B) shows a normal celiac origin (arrow). Spectral Doppler US images on inspiration (C) and expiration (D) demonstrates an abnormal peak systolic velocity of 318 cm/sec in expiration and a deflection angle of > 50 degrees.

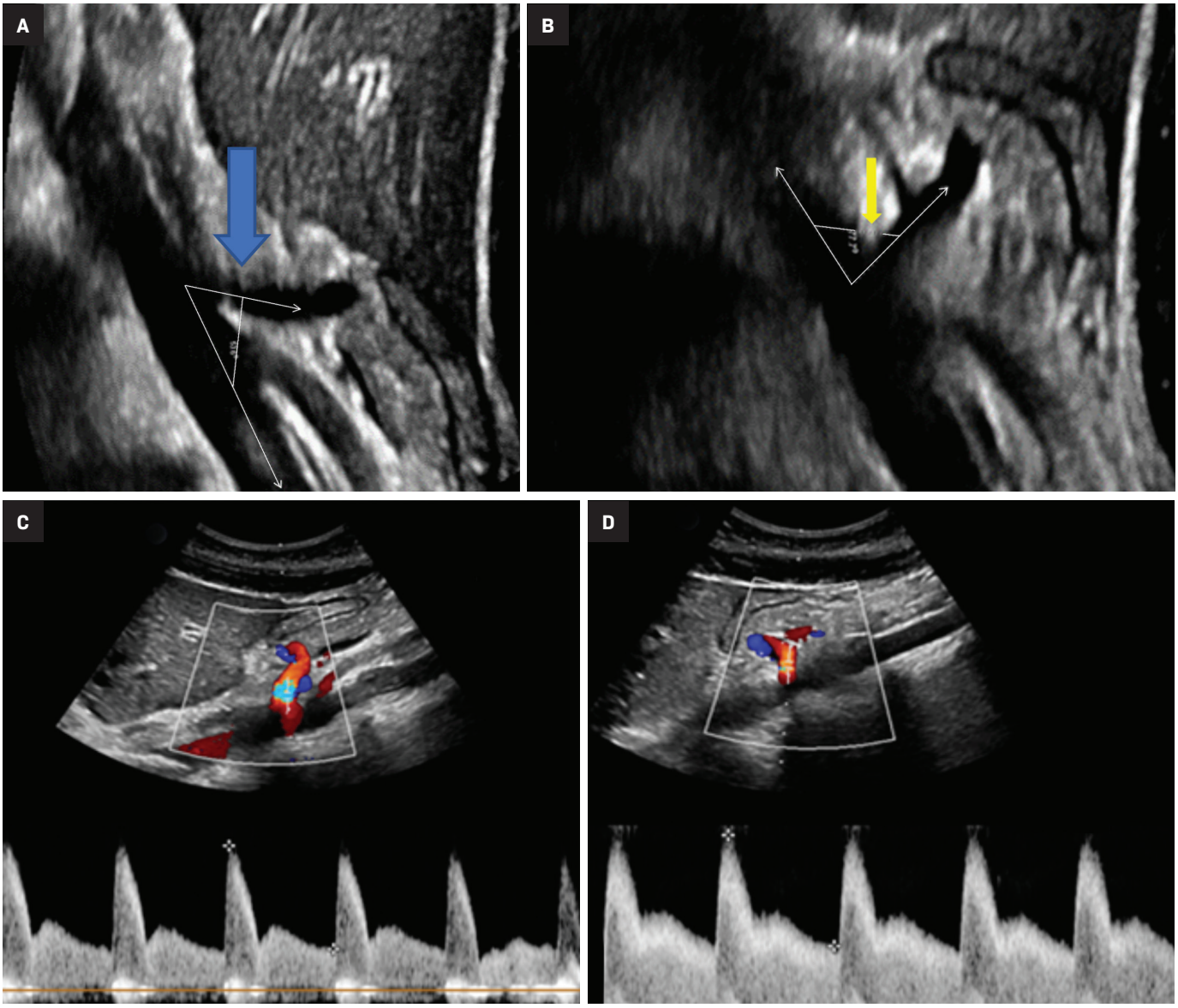

blood flow, suggesting celiac artery stenosis. As stenosis and/or compression occur the peak systolic velocity (PSV) increases, serving as a useful parameter for diagnosis. The PSV must be obtained at end inspiration, as in 13-51% of healthy individuals the celiac artery is compressed during expiration, although this is clinically insignificant.[3] During inspiration, the celiac trunk moves inferiorly in the abdominal cavity, relieving some of the compression and resulting in a lower PSV and potentially creating a false negative result. A peak systolic velocity of ≥200cm/s within the artery during expiration has a sensitivity of 75% and a specificity of 89% for MALS.[3]

Computed tomography scans with sagittal reconstruction are also useful in diagnosing MALS. Classic findings are narrowing and inferior displacement of the proximal celiac artery, forming a "J" shape or "hooking" of the artery. This helps to differentiate MALS from atherosclerosis in older adults. Catheter angiography is the gold standard for detecting arterial pathology, although CT angiography may obviate invasive imaging in most cases. Angiography may reveal post-stenotic dilation.

Management of MALS revolves around decompressing the celiac artery and the celiac plexus to restore blood flow and alleviate pain. Traditionally, open surgical decompression was the gold standard. The surgeon would dissect and separate the MAL fibers that were infringing on the celiac artery.[8] While the

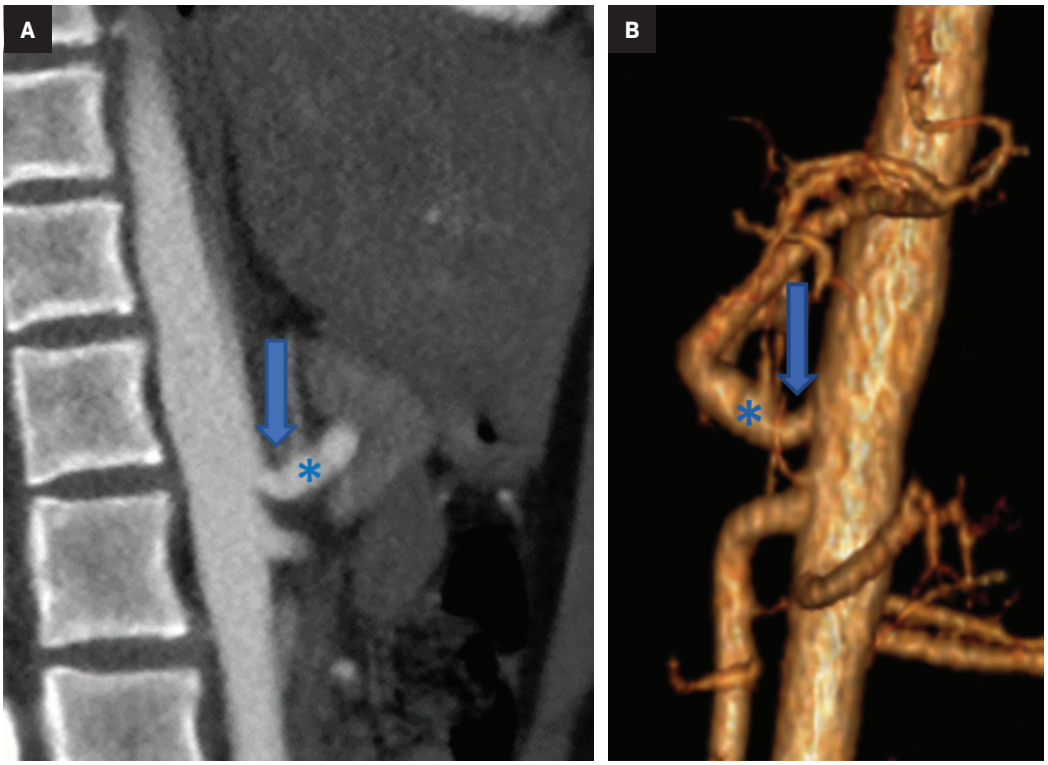

Figure 2. An abdominal CT angiogram (A) with 3D reconstruction (B) reveals arterial narrowing at the origin of the celiac axis (arrowhead) with post stenotic dilatation (*). Note the mild J-shape origin of the celiac artery.

procedure had a 0% 30-day mortality rate, it had a 16.1% complication rate. The most common complications were chylous ascites, pleural effusion, and wound dehiscence.[9]

More recently, laparoscopic surgery has become the preferred approach to treatment, as the procedure is minimally invasive, faster, (average 136 minutes), and requires a shorter hospital stay (average 3.8 days). Complications do occur with laparoscopic surgery, although at a lower rate than open surgery (5.1%).

A celiac plexus block (CPB) is another treatment option. In a study of 103 cases using CPB, 84% of patients reported lower post procedure pain scores, with the average score dropping from 6.3 to 0.9 on a 0-10 scale.[10] Nausea decreased from 37.9% before the procedure to 11.6% afterward. However, although CPB has a lower complication rate (0.97%) than laparoscopic surgery, it is not recommended for patients with ischemia, which cannot be corrected with the interventional procedure.[10]

Conclusion

Median arcuate ligament syndrome is important to keep in mind when presented with patient complaints of generalized abdominal symptoms, as it can lead to debilitating signs and symptoms, including marked weight loss. Obtaining Doppler ultrasound and sagittal CT scans at the end of inspiration is the most effective means of visualizing celiac artery compression. Laparoscopic surgery is typically the therapeutic option.

References

1) John H. Rodriguez. Median arcuate ligament syndrome: A clinical dilemma. *CCJM*. 2021; 88(3): 143-144.

2) mereczyński A, Kołaczyk K, Kiedrowicz R. New perspective on median arcuate ligament syndrome. Case reports. *J Ultrason*. 2021;21(86): e234-e236.

3) Narwani P, Khanna N, Rajendran I, Kaawan H, Al-Sam R. Median arcuate ligament syndrome diagnosis on computed tomography: what a radiologist needs to know. *Radiol Case Rep*. 2021;16(11):3614-3617.

4) Iqbal S, Chaudhary M. Median arcuate ligament syndrome (Dunbar syndrome). *Cardiovasc Diagn Ther*. 2021;11(5):1172-1176.

5) Vasiliadis HS, Teuscher R, Kleinschmidt M, Marrè S, Heini P. Temporary liver and stomach necrosis after lateral approach for interbody fusion and deformity correction of lumbar spine: report of two cases and review of the literature. *Eur Spine J*. 2016;;25 Suppl 1:257-266.

6) Scharf M, Thomas KA, Sundaram N, Ravi SJK, Aman M. Median arcuate ligament syndrome masquerading as functional abdominal pain syndrome. *Cureus*. 2021;13(12):e20573. doi:10.7759/cureus.20573

7) Lobst TP, Lamb KM, Spitzer SL, Patel RN, Alrefai SS. Median arcuate ligament syndrome. *Cureus*. 2022;14(2): e22106.

8) You JS, Cooper M, Nishida S, Matsuda E, Murariu D. Treatment of median arcuate ligament syndrome via traditional and robotic techniques. *Hawaii J Med Public Health*. 2013;72(8):279-281.

9) Duran M, Simon F, Ertas N, Schelzig H, Floros N. Open vascular treatment of median arcuate ligament syndrome. *BMC Surg*. 2017;17(1):95.

10) Barbon D, Hsu R, Noga J, Lazzara B, Miller T, Stainken B. Clinical response to celiac plexus block confirms the neurological etiology of median arcuate ligament syndrome. *JVIR*. 2021; 32(7): 1081-1087.

Sternoclavicular Physeal Separation

Kristie N. Nonyelu; Richard B. Towbin, MD; Carrie M. Schaefer, MD; Daniel Morgan, DO; Alexander J. Towbin, MD

Case Summary

A teenager presented with a brief history of right neck and trapezius pain after colliding with a classmate. On physical examination, the right sternoclavicular joint was tender to palpation and the right sternoclavicular joint was slightly depressed compared with the left side. The radial pulses were symmetric bilaterally, peripheral nerve function was intact.

Imaging Findings

An AP radiograph of the cervical spine (Figure 1) best showed the asymmetry in the appearance of the right and left sternoclavicular joints. A contrast -nhanced chest CT (Figure 2) showed the medial head of the right clavicle to be displaced posteriorly without fracture. There was no narrowing or disruption of the adjacent vessels.

Affiliations: University of Arizona College of Medicine-Phoenix Campus, Phoenix, Arizona (K. Nonyelu); Department of Radiology, Phoenix Children's Hospital, Phoenix, Arizona (Drs Schaefer, R. Towbin); Department of Radiology, University of Cincinnati College of Medicine (Drs Morgan, A. Towbin), Department of Radiology, Children's Hospital Medical Center, Cincinnati, (Dr A. Towbin).

Diagnosis

Sternoclavicular physeal separation

Discussion

Sternoclavicular joint (SCJ) dislocations are rare shoulder girdle injuries that comprise about 3% of all upper limb dislocations.[1–3] Because the medial aspect of the clavicle at the SCJ does not fully ossify until 23 to 25 years of life, most injuries are more correctly classified as physeal separations or fractures rather than true dislocations.[2,4,5] SCJ injuries are mostly seen in young, physically active males, engaged in contact sports.[4]

In older patients, anterior dislocation is 9 times more common. However, the incidence of anterior positioning in physeal separation is not known. The most common mechanisms causing posterior dislocations involve lateral compression of a flexed shoulder or direct force to the anteromedial aspect of the clavicle.[5]

A high degree of clinical suspicion is needed to make the diagnosis of an SCJ dislocation in a timely fashion.[2] In general, affected patients present with focal SCJ pain. They classically hold their arm in an adducted position with the elbow flexed and have limited ability to abduct the affected shoulder.[2,6] Additionally, patients prefer to rest with a flexed neck on the ipsilateral side and hold their elbow flexed with their contralateral arm.[6] Both maneuvers reduce strain on the affected SCJ.

Posterior SCJ dislocations are associated with injuries to mediastinal structures and subclavian vessels.[6,7] Knowledge of these injuries is used to help guide imaging protocols. Typically, imaging begins with chest and/or shoulder radiographs.[2] Supplemental views are often required for a diagnosis to be made with radiography.

Potentially useful views include the serendipity, Heinig, and Hobbs views.[6,8] The serendipity view is the most commonly performed of the three. In this view, a radiograph of the clavicles is obtained with 40 degrees of upward/cephalic tilt of the X-ray beam. If a posterior dislocation of the SCJ is present, the medial aspect of the dislocated clavicle is displaced inferiorly.[6] The Heinig view is a lateral view centered on the involved SCJ while the Hobbs view is obtained from an oblique posteroanterior approach.

Today, a contrast-enhanced CT of the chest should be performed whenever a SCJ dislocation is suspected clinically. CT is a sensitive modality

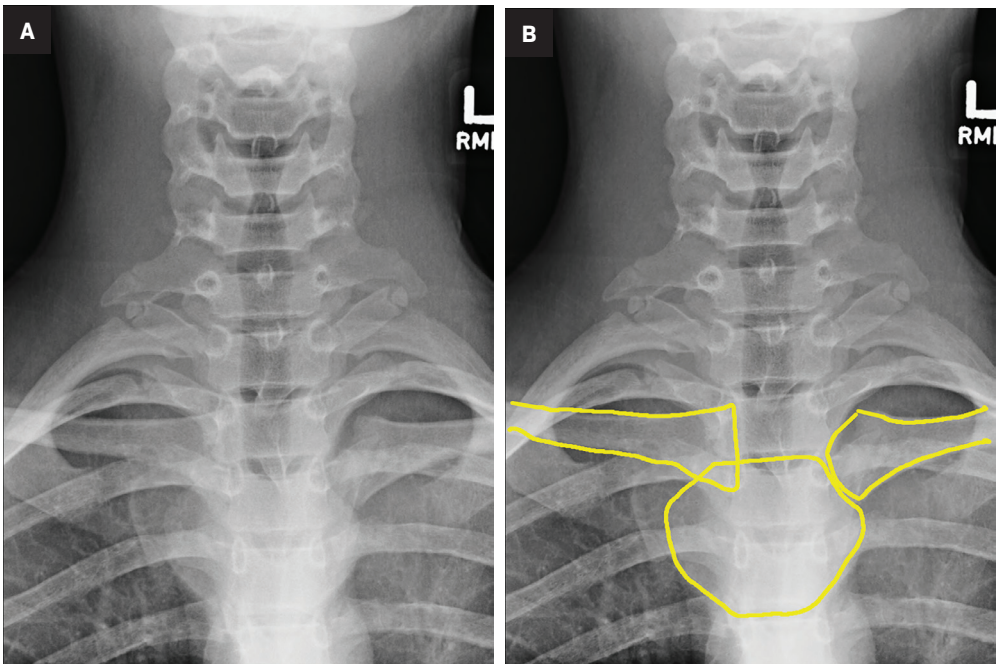

Figure 1. (A) AP radiograph of the cervical spine without and (B) with annotations shows superior displacement of the right sternoclavicular joint and overlap of the medial aspect of the sternum with the right lateral aspect of the manubrium.

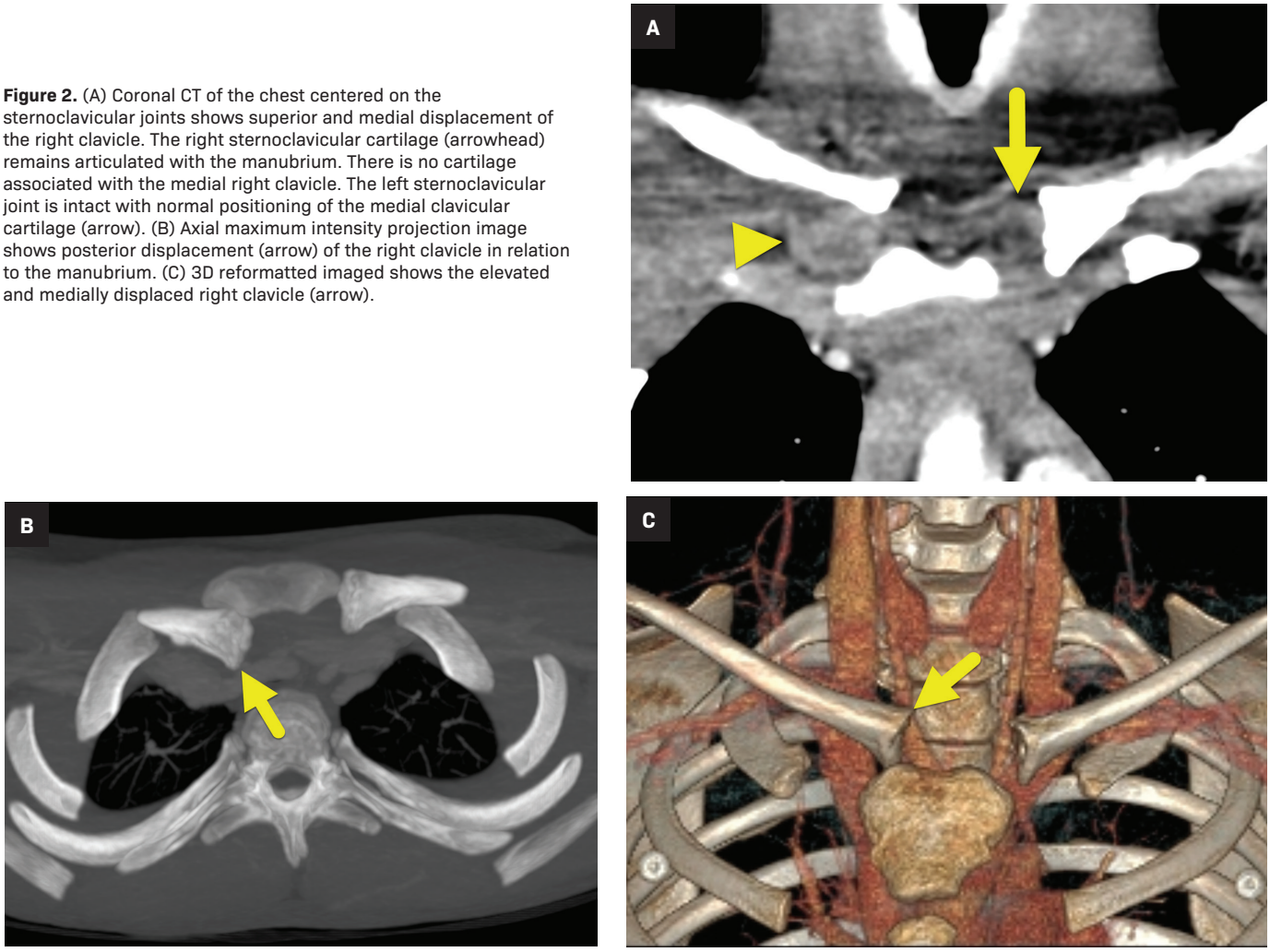

Figure 2. (A) Coronal CT of the chest centered on the sternoclavicular joints shows superior and medial displacement of the right clavicle. The right sternoclavicular cartilage (arrowhead) remains articulated with the manubrium. There is no cartilage associated with the medial right clavicle. The left sternoclavicular joint is intact with normal positioning of the medial clavicular cartilage (arrow). (B) Axial maximum intensity projection image shows posterior displacement (arrow) of the right clavicle in relation to the manubrium. (C) 3D reformatted imaged shows the elevated and medially displaced right clavicle (arrow).

to confirm the diagnosis and the extent of injury.[2] If there is a high degree of concern for a mediastinal injury, contrast-enhanced CT is used to assess the adjacent vasculature. Multiplanar and 3D reformatting can help distinguish sternoclavicular joint dislocations from physeal separations and can be used to guide surgical planning.[2] On CT, the cartilage appears slightly hypodense compared to soft tissue. In a separation, the cartilage remains next to the manubrium while in dislocations, the cartilage appears next to the medial aspect of the clavicle.

Most SCJ dislocations and physeal separations are treated with closed reduction within 7 to 10 days of injury.[1,5] Closed reduction requires the patient to be sedated to alleviate muscle spasms and intense pain.[1] During reduction, the patient lies supine with a foam pad positioned beneath the injured shoulder to position the shoulder posteriorly.[1] As the arm lies perpendicular to the body, sustained pressure is applied until the arm fully extends.[1] After treatment, the patient should avoid contact activities for 3 to 4 months.[1] Although closed reduction is more frequently recommended, open reduction is recommended if the patient presents outside of the 7-to-10-day window following injury, if there is neurovascular compression, or if the trachea or esophagus are injured.[1,5,7]

Complications including post-traumatic joint instability, osteoarthritis, and general joint dysfunction may occur.[3,8,9] These complications are less common in patients with posterior SCJ dislocations as compared to those with anterior dislocations.[1] Our patient was treated with open reduction and internal fixation to stabilize the physeal separation.

Conclusion

The diagnosis of posterior SCJ dislocations requires a high degree of clinical suspicion to make the diagnosis. Chest and sternoclavicular radiographs are the often the initial step, but CT scans are the diagnostic modality of choice. Early intervention can help prevent long term disability.

References

1) Garcia JA, Arguello AM, Momaya AM, Ponce BA. Sternoclavicular joint instability: symptoms, diagnosis and management. *Orthop Res Rev*. 2020;12:75-87. doi: 10.2147/ORR.S170964. PMID: 32801951; PMCID: PMC7395708.

2) Chaudhry, Sonia. Pediatric Posterior Sternoclavicular Joint Injuries. *JAAOS - J Am Acad Orthop Surg*. 2015;23(8):468. doi:10.5435/JAAOS-D-14-00235

3) Warnhoff M, Lill H, Jensen G. CME Zertifizierte Fortbildung Verletzungen des Sterno-klavikulargelenks Rony-Orijit Dey Hazra · Anne-Rieke Reich · Marek Hanhoff ·. *Unfallchirurg*. 2020;123:879-889. doi:10.1007/s00113-020-00888-2

4) Robinson CM, Jenkins PJ, Markham PE, Beggs I. Disorders of the sternoclavicular joint. *J Bone Jt Surg - Ser B*. 2008;90(6):685-696. doi:10.1302/0301-620X.90B6.20391/ASSET/IMAGES/LARGE/20391-8B.JPEG

5) Sewell MD, Al-Hadithy N, Le Leu A, Lambert SM. Instability of the sternoclavicular joint: Current concepts in classification, treatment and outcomes. *Bone Jt J*. 2013;95 B(6):721-731. doi:10.1302/0301-620X.95B6.31064/ASSET/IMAGES/LARGE/31064-GALLEYFIG6C.JPEG

6) Carius BM, Long B, Gottlieb M. Evaluation and management of sternoclavicular dislocation in the emergency department. *J Emerg Med*. 2021;61(5):499-506. doi:10.1016/J.JEMERMED.2021.07.038

7) Kraus R, Zwingmann J, Jablonski M, Bakir MS. Dislocations of the acromioclavicular and sternoclavicular joint in children and adolescents: A retrospective clinical study and big data analysis of routine data. *PLoS One*. 2020;15(12). doi:10.1371/JOURNAL.PONE.0244209

8) Rudzki JR, Matava MJ, Paletta GA. Complications of treatment of acromioclavicular and sternoclavicular joint injuries. *Clin Sports Med*. 2003;22(2):387-405. doi:10.1016/S0278-5919(03)00013-9